

Spt6 Regulates Intragenic and Antisense Transcription, Nucleosome Positioning, and Histone Modifications Genome-Wide in Fission Yeast

Christine M. DeGennaro,^a Burak H. Alver,^b Samuel Marguerat,^{c*} Ekaterina Stepanova,^a Christopher P. Davis,^a Jürg Bähler,^c Peter J. Park,^{b,d} Fred Winston^a

Department of Genetics, Harvard Medical School, Boston, Massachusetts, USA^a; Center for Biomedical Informatics, Harvard Medical School, Boston, Massachusetts, USA^b; Department of Genetics, Evolution, and Environment and UCL Cancer Institute, University College of London, London, United Kingdom^c; Division of Genetics, Department of Medicine, Brigham and Women's Hospital, Boston, Massachusetts, USA^d

Spt6 is a highly conserved histone chaperone that interacts directly with both RNA polymerase II and histones to regulate gene expression. To gain a comprehensive understanding of the roles of Spt6, we performed genome-wide analyses of transcription, chromatin structure, and histone modifications in a *Schizosaccharomyces pombe* *spt6* mutant. Our results demonstrate dramatic changes to transcription and chromatin structure in the mutant, including elevated antisense transcripts at >70% of all genes and general loss of the +1 nucleosome. Furthermore, Spt6 is required for marks associated with active transcription, including trimethylation of histone H3 on lysine 4, previously observed in humans but not *Saccharomyces cerevisiae*, and lysine 36. Taken together, our results indicate that Spt6 is critical for the accuracy of transcription and the integrity of chromatin, likely via its direct interactions with RNA polymerase II and histones.

Studies over the last few years have revealed that transcription across eukaryotic genomes is much more widespread and complex than previously believed (1). Although it was once thought that transcription occurs primarily across protein-coding regions, genome-wide studies have now shown that transcription is also prevalent in intergenic regions and on antisense strands, in organisms ranging from yeast to humans (2, 3). Although roles for a small amount of this transcription have been established, for most, we have little understanding of its biological functions. Furthermore, while some factors have been shown to control the level of noncoding and antisense transcripts, many questions remain regarding the regulation of their synthesis and stability.

One factor that plays a prominent role in the genome-wide control of transcription is Spt6. Originally identified in *Saccharomyces cerevisiae* (4, 5), Spt6 is conserved throughout eukaryotes and also has homology to the prokaryotic activator Tex (6). Spt6 interacts directly with several important factors, including RNA polymerase II (RNAPII) (7–11), histones (12, 13), and the transcription factor Iws1/Spn1 (7, 14, 15), suggesting that it is multifunctional. Recent studies in mammalian cells show that Spt6 also interacts directly with other chromatin related factors, including H3K27 demethylases (16, 17). Several gene-specific studies have demonstrated roles for Spt6 in transcription initiation (18–20), elongation (21, 22), and termination (23, 24). In addition, Spt6 is required for H3K36 methylation (25–28) and regulates nucleosome positioning and occupancy, particularly over highly expressed genes (12, 19, 29). Finally, Spt6 can assemble nucleosomes *in vitro* in an ATP-independent fashion (12). These results suggest that Spt6 acts as a histone chaperone by restoring nucleosomes in the wake of RNAPII transcription (30, 31).

In vivo, Spt6 is critical for normal growth and transcription. It is either essential or nearly essential for viability in all organisms tested, and viable *spt6* mutations cause severe defects. In *S. cerevisiae* *spt6* mutants, transcription is greatly altered, as cryptic intragenic transcription is widespread (32), and in *Schizosaccharomyces pombe* *spt6* mutants, all forms of heterochromatic silencing are impaired (33, 34). In addition, *spt6* mutations cause developmen-

tal defects in both *Caenorhabditis elegans* (35) and zebrafish (36). Studies in mammalian cells show that Spt6 is an important global regulator of transcription, including of genes implicated in cancer and viral infection, such as HIV and cytomegalovirus (CMV) (13, 17, 27, 37–39).

Taken together, the documented effects of Spt6 on transcription and chromatin regulation are diverse and extensive. To more comprehensively understand the global roles of Spt6 *in vivo*, we have now systematically studied the genome-wide effects of Spt6 on transcription, chromatin structure, and three histone modifications in *S. pombe*. Our results reveal that Spt6 is broadly required for normal transcription and chromatin structure. In an *spt6* mutant, transcription is altered genome-wide, including changes to the levels and start sites of mRNAs, as well as elevated levels of intragenic and antisense transcripts. In addition, nucleosome occupancy and phasing over transcribed regions are disrupted, and two histone modifications, H3K4me3 and H3K36me3, are reduced to background levels. The extensive defects that we observe in an *spt6* mutant reveal that Spt6 is a master regulator of transcription and chromatin in *S. pombe*, and current evidence suggests that these roles are likely conserved throughout eukaryotes.

MATERIALS AND METHODS

***S. pombe* strains and genetic manipulations.** The *S. pombe* strains used in the present study are listed in Table S1 (available at <http://goo.gl/OEGSsQ>). Unless otherwise indicated, strains were cultured at 30°C, using yeast extract supplemented (YES) medium, and crosses and tetrad dissection

Received 15 August 2013. Returned for modification 14 September 2013

Accepted 27 September 2013

Published ahead of print 7 October 2013

Address correspondence to Fred Winston, winston@genetics.med.harvard.edu.

* Present address: Samuel Marguerat, Quantitative Gene Expression Group, MRC Clinical Sciences Centre, Imperial College London, London, United Kingdom.

Copyright © 2013, American Society for Microbiology. All Rights Reserved.

[doi:10.1128/MCB.01068-13](https://doi.org/10.1128/MCB.01068-13)

were performed as previously described (40). Gene deletions and epitope tagging were performed by homologous recombination of PCR-generated DNA sequences into the genome. PCR primers contained 80 bases of homology to the genome and 20 bases for amplification from previously described plasmids (41). For gene deletions, a *KanMX6* or *NatMX6* cassette was targeted to sites flanking the open reading frame. For epitope tagging, cassettes encoding the tag and marked by *KanMX6* or *NatMX6* were integrated at the 3' end of the gene, removing the endogenous stop codon. All epitope-tagged genes are still functional, based on phenotype analysis. We note that an epitope-tagged version of Set1 was not used in analysis of the COMPASS complex, as tagging abolished Set1 function. All deletions, promoter insertions and tags were verified by PCR analysis. Tags were also verified by Western blotting with a peroxidase antiperoxidase (PAP) antibody (Sigma) for TAP tags, an anti-Myc antibody (A14; Santa Cruz Biotechnology), an anti-Flag antibody (M2; Sigma), or an antihemagglutinin (anti-HA) antibody (12CA5; Abcam). Ponceau red staining or antitubulin signal (sc-53030; Santa Cruz) was used to determine whether equal amounts of protein were loaded in each lane. All of the primers used for strain construction are listed in Table S2 (available at <http://goo.gl/OEGSsQ>).

Transcriptome library preparation and sequencing. RNA was prepared by acid-phenol extraction as previously described (43), from prototrophic wild-type and *spt6-1* strains shifted to 37°C for 2 h. Portions (10 µg) of total RNA were used as starting material for strand-specific library preparation using the Illumina Universal RNA-seq samples prep kit. This kit was an unreleased early version provided by Illumina of the Illumina TruSeq small RNA sample preparation kit. Briefly, poly(A)⁺ RNA was enriched by two rounds of poly(dT) Sera-Mag magnetic beads purification and then fragmented to an average size of ~200 nucleotides. Fragmented RNA was 3' dephosphorylated with Antarctic phosphatase and 5' phosphorylated with polynucleotide kinase to prepare RNA fragments for subsequent ligation. Illumina RNA adaptors were ligated to the 5' and 3' ends using a 3' RNA ligase and a T4 RNA ligase, respectively. First-strand cDNA was produced using a primer specific for the Illumina 3' adaptor. The library was amplified with 15 cycles of PCR using primers specific for the Illumina adaptors and purified by using SPRI-beads (Agencourt; Beckman Coulter). Library size distributions and concentrations were determined on an Agilent Bioanalyzer. RNA-seq libraries were sequenced on an Illumina Genome Analyzer IIx instrument.

RNA-seq data processing. The sequenced reads from each sample were aligned in two steps using TopHat (44) to *S. pombe* genome assembly ASM294v2 with default parameters, except for the intron length range of 30 to 2,000 bp (“-i 30 -I 2000” options). In the first round, no annotation guide was provided. The splice junctions that were discovered for the four samples were merged with annotated splice junctions (ASM294v2.18) to obtain a complete list of splice candidates. In the second round of alignment, these junctions were provided as a guide to the aligner (“-j <junction file>, -no-novel-juncs” options). The reads per kilobase per million mapped read (RPKM) score was calculated for each transcription unit on the sense and antisense strands; sense scores reflected only exonic reads, whereas the complete transcription unit was used in the antisense direction. Different samples were normalized relative to each other to account for differences in the ratios of antisense and intergenic reads, intron retention rates, and t/rRNA filtering efficiency. The RPKM values for each of the samples was scaled by a linear factor, such that the mode of the log fold change distribution for sense RPKM values between each sample and the average of the four samples was “0.” The linear factor was between 0.75 and 1.1 for the four samples. A high degree of reproducibility was observed between replicates. Genes were considered to be 2-fold enriched only if they were 2-fold enriched in both replicates. The final RPKM values are presented as linear averages between replicates (see Table S3 at <http://goo.gl/OEGSsQ>). A continuous RNA-seq signal was calculated at single-base-pair resolution for the whole genome as follows: RNA signal = (number of reads covering the position)/(total number of aligned reads)/(read length in sample) × (normalization factor determined using RPKM

values above) × 10¹⁰. This measure corresponds roughly to 10·RPKM at each position and was found to be optimal in representing the data when a pseudocount of 1 is introduced. The RNA-seq metagene plots and browser screenshots present log₂(linear RNA signal + 1). The final logged RNA-seq signal was averaged between replicates.

To compare RNA-seq data to previous microarray data, the microarray probes (45–47) were mapped to ASM294v2, and only the uniquely aligning probes were preserved. The logged RNA-seq signal values for wild-type (WT) and *spt6-1* samples were then averaged for each probe within ±20 bp of the probe. The log fold change values were calculated for each “probe” as (*spt6-1* – WT) and averaged over the two replicate pairs. A total of 362 coding genes with no antisense annotations covered by at least five microarray probes were selected. The average antisense signal was calculated for each gene. Pearson *r* values were calculated between each sample pair based on the antisense signal change relative to the WT. The different mutants were clustered hierarchically using the Euclidean distance between *r* values as a distance measure.

Grayscale heat maps for genes were generated based on the log₂ RNA-seq signal. For genes longer than 4 kb, only the 5' and 3' 2-kb ends of the genes are presented. The sense strand signal was aligned at the 5' transcription start site (TSS), whereas the antisense strand signal was aligned at the transcription termination site (TTS). The metagene profiles present averages for genes longer than 700 bp. The 3' and 5' 350 bp of the metagene profiles present averages over the 3' and 5' ends of all genes. The points in the middle of the metagene profiles present average values across genes that are long enough to have signal at the given position; for example, the value at 1 kb is the average across genes longer than 1,350 bp in the sense direction. Similarly, the value at 3 kb (TTS – 1 kb) is an average across genes longer than 1,350 bp for the antisense profile, since the antisense profiles are aligned at the 3' end. The linear scale RNA-seq signal metagene plots were obtained in a similar way, where instead of an average over all genes, a trimmed mean (0.1 to 0.9) is presented to remove genes with extreme values.

The final numbers on splice junctions were based on junctions that were observed in both replicates for a given condition (WT or *spt6-1*) and that had >50% reads supporting the junction rather than intron retention. The branch point consensus sequence was calculated using the sequence motif search tool MEME (48), with over 1,000 randomly selected intron sequences as a 5-bp motif (“-minw 5 -maxw 5” options). The presence of the branch point consensus sequence in an intron was evaluated using MAST (48) with *P* < 0.01 (“-mt 0.01” option). The consensus sequence was required to be in the 30-bp 3' end of the intron in the correct orientation.

The presence of cryptic intragenic initiation events in the sense direction inside gene bodies would result in the increase of RNA-seq signal toward the 3' ends of genes. To assess cryptic sense initiation, we calculated a 3' enrichment score as follows. For each base pair position along a gene starting at the 3' end, the number of reads between the given position and the 3' end of the gene was counted. The value for *spt6-1* samples was plotted against the value for WT. If there is no cryptic initiation event, the curve described should increase roughly linearly. However, if there are cryptic initiation events, the value for *spt6-1* will be higher than the WT value, relative to diagonal, for most positions along the gene. The ratio of the area under the described curve to the area under the diagonal is given as the 3' enrichment score (see Fig. S4B at <http://goo.gl/OEGSsQ>). For 1-kb subgene analysis, the same analysis was repeated using only the most central 1 kb of each gene. For comparison of replicates, we calculated the 3' enrichment score of combined second replicates (WT II and *spt6-1* II) relative to first replicates (WT I and *spt6-1* I). For all analyses, similar qualitative results were obtained when the analyses were performed on the individual experiments. The combined results are presented.

Strand specific reverse transcription-qPCR analysis. RNA was prepared as described above from WT and *spt6-1* strains grown at 30°C. RNA samples were treated with the Turbo DNase kit (Invitrogen) and reverse transcribed with strand-specific primers using Superscript III (Invitro-

gen). cDNA was analyzed by quantitative PCR (qPCR) on the Stratagene MX3000P cycler. Each sample was run in quadruplicate and quantified by comparison to a standard curve (10-fold serial dilutions of a sample). Primers used for qPCR amplification are listed in Table S2 (available at <http://goo.gl/OEGSsQ>).

Nucleosome positioning by MNase-seq. MNase-seq libraries were prepared as previously described with minor modifications (49). Briefly, cells from strains FWP172 (WT) and FWP371 (*spt6-1*) were grown in 200 ml of YES medium to an optical density at 600 nm of 0.5, shifted to the nonpermissive temperature of 37°C for 2 h, cross-linked for 10 min using 1% formaldehyde, quenched for 5 min by 125 mM glycine, harvested, and washed twice with ice-cold water. Cells were spheroplasted in 2 ml of CES buffer (50 mM citric acid–50 mM Na₂HPO [pH 5.6], 40 mM EDTA [pH 8.0], 1.2 M sorbitol) containing 1 mg of Zymolyase 100T (U.S. Biologicals)/ml and 20 mM β-mercaptoethanol for 1 h at 30°C. Spheroplasts were pelleted, washed with 50 ml of Tris-sorbitol buffer (40 mM Tris-HCl [pH 8.0], 1.2 M sorbitol, 50 mM NaCl, 1 mM EDTA), and subjected to MNase digestion in 2 ml of NP buffer (40 mM Tris-HCl [pH 8.0], 1.2 M sorbitol, 50 mM NaCl, 1 mM EDTA, 0.1% Nonidet P-40, 0.75% Sigma fungal protease inhibitor cocktail, 10 mM β-mercaptoethanol, 5 mM spermidine, 10 mM CaCl₂) containing 150 U of nuclease S7 (Roche)/ml for 5 min at 37°C. Reactions were stopped by the addition of an EDTA and EGTA mix to final concentrations of 25 mM each. Cross-linking was reversed overnight at 65°C in the presence of 0.5% sodium dodecyl sulfate (SDS) and 1 mg of proteinase K/ml. DNA was purified by phenol-chloroform extraction and ethanol precipitation. RNA was removed by treatment with RNase A/T₁ mix (Fermentas). Purified DNA was resolved on 1% agarose gel, and a band corresponding to mononucleosomal fragments was excised and subjected to gel extraction. Gel-purified DNA was used for building sequencing libraries using procedures analogous to those used for preparation of ChIP-seq libraries.

The sequenced reads were aligned by using Bowtie allowing up to 10 matches (“-m 10 -best” options). Paired-end sequenced fragments with an inferred length between 90 and 200 bp were kept for downstream analysis. A home-brew GC-content normalization, similar to BEADS, was applied to reduce variability in GC content of different samples. Instead of normalizing all samples to a flat GC distribution, the normalization brought the GC content of all samples similar to one of the samples, deemed to be midway. The final conclusions were independent of this normalization procedure. The MNase-seq profile was calculated using a Gaussian Kernel smoothing (bandwidth = 20 bp) on the positions of the paired-end fragment centers. Metagene profiles were prepared similar to the sense-strand RNA-seq profiles from the smoothed MNase-seq profiles. Replicates were averaged.

Histone modification Western blots. Proteins were extracted in the presence of trichloroacetic acid, electrophoresed on 3.75 to 15% SDS-PAGE gels, and transferred to Immobilon-P membrane. Membranes were incubated with anti-H3 (ab1791; Abcam), anti-H3K4me3 (ab8580; Abcam), anti-H3K36me3 (ab9050; Abcam), anti-H2B (ab1970; Abcam), or anti-H2BK120ub (39623; Active Motif) and then with antitubulin (sc-53030; Santa Cruz). Ponceau red staining and tubulin signal was used to determine equal loading.

ChIP. Chromatin immunoprecipitation (ChIP) experiments were performed as described previously (50). Briefly, 100-ml cultures grown to 1×10^7 to 2×10^7 cells/ml were cross-linked (1% formaldehyde, 30 min) and lysed by bead beating. The chromatin fraction was isolated and sheared to 200- to 500-bp fragments using a Bioruptor sonicator (Diagenode) or Sonicator 3000 (Misonix). Immunoprecipitations (IPs) were performed overnight at 4°C with 1 µg of anti-H3 (ab1791; Abcam), 2 µg of anti-H2B (ab1970; Abcam), 3 µg of anti-H3K36me3 (ab9050; Abcam), 5 µg of anti-H3K4me3 (ab8580; Abcam), 5 µl of anti-Rpb1 (8WG16; Covance), 5 µl of anti-HA (ab9110; Abcam), or 5 µl of anti-Myc (9E10; Santa Cruz Biotechnology). IPs were coupled to 50 µl of protein G-Sepharose beads (GE Healthcare Life Sciences) at 4°C for 4 h. The beads were washed and eluted, and the eluate was reverse cross-linked overnight at

65°C and incubated with proteinase K and glycogen for 2 h at 37°C. DNA was purified by phenol-chloroform extraction and precipitated in ethanol overnight at -20°C. ChIP DNA was analyzed by qPCR on the Stratagene MX3000P cycler. Each sample was run in triplicate and quantified by comparison to a standard curve (10-fold serial dilutions of input DNA). The primers used for qPCR amplification are listed in Table S2 (available at <http://goo.gl/OEGSsQ>). Relative percent IP (%IP) values for some experiments were calculated by dividing the %IP (calculated as IP/input) at the regions of interest by the %IP at a previously described intergenic background locus (*gfr*) (51) or the region upstream of the *act1*⁺ transcription start site (TSS). For all of the histone modifications, the %IP was normalized to the %IP of H3 or H2B. The specificity of enrichment was determined by analysis of either an untagged or no antibody control, but these were not used for normalization.

ChIP library building, sequencing, and analysis. Between 1 and 10 ng of ChIP DNA were processed for each ChIP-seq library. DNA was end repaired with T4 DNA polymerase (Invitrogen), T4 PNK (NEB), and DNA polymerase I, large Klenow fragment (Invitrogen), and an “A” base was added using Klenow 3' to 5' exo minus (NEB). Then, 1-pmol portions of barcoded adaptors were ligated on with T4 DNA ligase (Roche), and the products were PCR amplified with Phusion DNA polymerase (NEB) and size selected by purification on 2% agarose-EX E-gels (Invitrogen) for fragments between 200 and 600 bp. The library size and concentration were determined by using Bioanalyzer or Tapestation analysis (Agilent), and libraries were pooled in equimolar amounts with up to 26 in each sequencing lane. Pooled libraries were gel purified twice, followed by column purification on MinElute columns (Qiagen). Samples of at least 10 nM were submitted for analysis on the Illumina Hi-Seq at Tufts University Core Facility.

The sequenced reads were aligned using Bowtie (52), allowing up to 10 matches (“-m 10 -best” options). To correct for any variability in GC-content bias between IP and input samples, the samples were processed with BEADS (53). For BEADS processing, the fragments were extended in the 3' end direction to be 100 bp long, which is the typical fragment length for our samples inferred from cross-correlation results (“beads extend -threePrim <100-read length>”). Spp (54)-defined broad enrichment clusters ($z = 3$) were excluded in the BEADS calculation. Downstream ChIP-seq analysis was performed on BEAD-processed profiles in 10-bp bins (“beads tagCount -base 10”). The input signal was calculated conservatively as the maximum of the signal in the given bin, the average signal in a 100-bp region surrounding the bin, or half of the genome-wide average input signal. The IP enrichment was calculated as the ratio of IP signal to the input signal at each bin. The enrichment signal was linearly normalized such that the median enrichment value for the whole genome is set to 1. All qualitative conclusions were evaluated with each replicate separately. The final results show signal averaged from two replicates. Metagene profiles for ChIP-seq were obtained similarly to the sense strand RNA-seq results, aligning all genes at 5' end using genes longer than 700 bp. An average gene enrichment score was calculated for each sample and is presented on scatter plots. These values were calculated using the total BEADS corrected and normalized tag count for IP and input samples. For Swd1 and H3K4me3, the enrichment was calculated at the first 500 bp from the 5' end. For H3 and H2B, the whole gene body was used, and for Spt6, Rpb1, Ctr9, Set2, and H3K36me3, the gene body excluding the first 500 bp was used. Only genes with more than a normalized input tag count of 5 were included in the scatter plot for each sample to remove genes with potentially high statistical fluctuations.

Data accession number. The data discussed in this publication have been deposited in NCBI's Gene Expression Omnibus (GEO) (42) and are accessible through GEO series accession number [GSE49575](https://www.ncbi.nlm.nih.gov/geo/query/acc.cgi?acc=GSE49575).

RESULTS

Antisense and intragenic transcripts are greatly elevated in an *S. pombe* *spt6* mutant. To characterize the role of Spt6 in transcription at high resolution, we performed strand-specific RNA-seq,

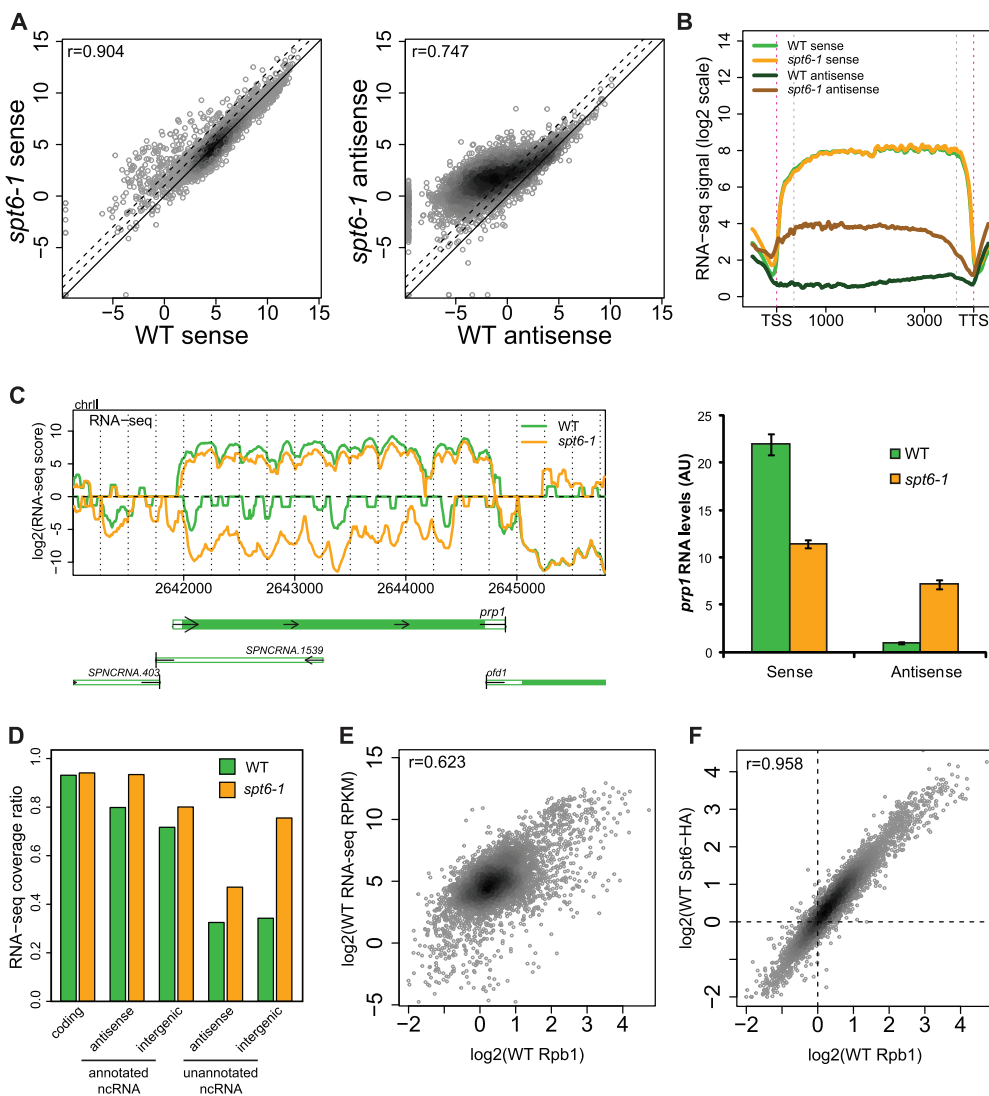


FIG 1 *Spt6* is required globally for transcriptional accuracy. (A) Sense (left panel) and antisense (right panel) \log_2 RPKM scores are plotted for each transcription unit for *spt6-1* versus WT, with the indicated r value corresponding to the Pearson correlation. The solid line indicates no change, and dashed lines correspond to 2- and 4-fold increases. (B) Metagene analysis of the WT and *spt6-1* \log_2 RNA-seq signal on the sense and antisense strands aligned to the transcription start site (TSS) and transcription termination site (TTS), indicated by the pink dashed lines. For all metagene figures, the first and last 350 bp within the transcription unit (indicated by gray dashed lines) are calculated from all genes, while the remainder of the metagene is calculated as an average of all genes with length up to the given position. (C) Validation of the RNA-seq data for the *prp1*⁺ gene (left panel) by strand-specific RT and qPCR (right panel). For the RNA-seq data, the top panel represents the plus strand (positive values), and the bottom panel represents the minus strand (negative values) \log_2 (RNA-seq scores) over the *prp1*⁺ region. For the qPCR data, each bar represents the mean \pm the standard error of the mean (SEM; $n = 4$), in arbitrary units (AU), normalized to the antisense levels in the WT strain. (D) The genome coverage was determined from the pooled replicates of WT and *spt6-1* samples with equal sequencing depth. At this depth, the coverage of each class of transcript is indicated by the bars. (E) The WT \log_2 sense RPKM scores are plotted against the \log_2 Rpb1 ChIP-seq enrichment scores for each transcription unit, with the indicated r value corresponding to the Pearson correlation. (F) The WT \log_2 ChIP-seq enrichment scores are plotted for Rpb1 and hemagglutinin (HA)-tagged Spt6 in a WT strain, with the indicated r value corresponding to the Pearson correlation.

comparing the WT to an *spt6-1* mutant. Although the *spt6⁺* gene is not essential for viability in *S. pombe*, an *spt6Δ* mutant grows extremely slowly, taking several days to form a colony (34). Therefore, we used the well-characterized *spt6-1* temperature-sensitive allele, which has been previously shown to confer strong phenotypes (34). The RNA-seq experiment was performed twice, with similar results each time (see Fig. S1 at <http://goo.gl/OEGSsQ>); all of the described effects were observed in both experiments. We observed a number of changes in the expression of annotated coding regions (Fig. 1A), with increased RNA levels for 373 genes and

decreased levels for 114 genes, at a >2-fold change. Many of the genes with increased RNA levels are lowly expressed. A large subset of these are located in heterochromatinized subtelomeric regions that are desilenced in the *spt6-1* mutant, as we observed previously (34). However, the more striking change was to antisense transcript levels (Fig. 1A and B), with 3,700 of 5,123 genes (72%) displaying a >2-fold increase; over half (1,895) of these antisense transcripts occur within genes without any previously annotated antisense transcripts. Thus, a number of novel antisense transcripts are present in the *spt6-1* mutant, as was recently

observed in *S. cerevisiae* (55). To validate the RNA-seq data, we measured sense and antisense transcript levels using strand-specific reverse transcription, followed by quantitative real-time PCR (qPCR) for two genes that appeared affected and one that did not (Fig. 1C; see also Fig. S2A at <http://goo.gl/OEGSsQ>) and found similar results, confirming the increase in antisense transcription that was detected by RNA-seq.

Overall, we observed an increase in the portion of the genome transcribed, with 63% transcribed in the WT and 80% transcribed in the *spt6-1* mutant at the same sequencing depth, and excluding tRNA, rRNA, and other nonunique regions (see Fig. S2B at <http://goo.gl/OEGSsQ>). Some of this increase in coverage comes from annotated antisense and intergenic noncoding RNA, since their coverage increased from 80 to 93% and from 72 to 80%, respectively (Fig. 1D). The rest of the increase is due to previously unannotated antisense and intergenic regions, which show increases in coverage from 33 to 47% and from 34 to 76%, respectively (Fig. 1D). In contrast, coverage of coding regions is similar, with 93% in the WT and 94% in the *spt6-1* mutant. Taken together, these results suggest that transcription is substantially more pervasive in the *spt6-1* mutant and therefore indicate that Spt6 is required for transcriptional accuracy in *S. pombe*.

Given the changes to transcription in the *spt6-1* mutant, we compared the level of association of the Rpb1 subunit of RNAPII in WT and *spt6-1* strains. Overall, the Rpb1 enrichment is similar in the WT and *spt6-1* strains (see Fig. S3 at <http://goo.gl/OEGSsQ>) ($r = 0.94$, Pearson correlation), which is likely reflective of similar amounts of sense transcription in the two strains (Fig. 1A). Although antisense transcript levels are increased globally, if our RNA-seq data primarily reflect the level of RNA synthesis, the majority of transcription still occurs on the sense strand, and this dominates the Rpb1 recruitment data. In agreement with this, we observed good correlation between the Rpb1 recruitment and sense transcript level (Fig. 1E) ($r = 0.62$, Pearson correlation), with noise likely due to RNA stability. We also observed a strong correlation between Rpb1 and Spt6 binding over transcribed regions (Fig. 1F) ($r = 0.96$, Pearson correlation; see also Fig. S3A and B at <http://goo.gl/OEGSsQ>). Overall, these data support the observed transcriptional effects and suggest that Spt6 is recruited with RNAPII to sites of active transcription and plays a direct role in maintaining transcriptional accuracy.

In *S. pombe*, two main pathways have been implicated in the repression of antisense transcripts: first, the RNA interference (RNAi) machinery, the exosome, and H2A.Z have been shown to play a role in transcriptional and posttranscriptional repression of readthrough transcription at convergent genes, and second, the Set2 histone H3 lysine 36 (H3K36) methyltransferase, the Clr6 histone deacetylase complex, and the Chd1 chromatin remodelers (Hrp1 and Hrp3) are important for the repression of cryptic intragenic transcription initiation (45–47, 56–61). To determine whether Spt6 fits into either of these pathways, we compared our *spt6-1* RNA-seq data with tiling array data from previous studies. We found that antisense transcription in the *spt6-1* mutant clusters most closely with mutants in the Clr6 complex, *set2Δ*, and *hrp3Δ* (Fig. 2A; see also Table S4 and Fig. S4A at <http://goo.gl/OEGSsQ>), a finding consistent with the fact that genes with increased antisense levels in the *spt6-1* mutant are not enriched for convergent genes. Instead, we found that the majority of the antisense transcripts arose from within genes (Fig. 2B), independently of the orientation relative to adjacent genes (Fig. 2C). The increase

in transcript level across the gene body was linear (Fig. 2C), suggesting that the antisense transcripts originate from cryptic promoters randomly distributed across the gene. Taken together, these results suggest that the majority of antisense transcripts in the *spt6-1* mutant are derived from intragenic initiation events.

We also investigated whether there was evidence for intragenic transcription initiation on the sense strand, as there is in *S. cerevisiae* (29, 32). This is more difficult to assess, since the higher level of sense transcripts can obscure detection of novel initiation within a gene (32, 62) (Fig. 2D). To measure intragenic transcription, we calculated a 3' enrichment score (see Materials and Methods; see also Fig. S4B at <http://goo.gl/OEGSsQ>) for all genes and found an increased 3' enrichment in the *spt6-1* mutant compared to the WT, which increased with the length of the gene (Fig. 2E), suggesting that there are transcripts initiating from within the gene body. We performed, as a control, the same analysis between the replicates, with pooled WT and *spt6-1* data in each set (Fig. 2E). As expected, the control analysis showed no 3' enrichment of the RNA-seq signal between replicates. In order to determine whether the dependence of 3' enrichment on gene length was associated with a higher frequency of intragenic initiation in longer genes or a higher likelihood of observing intragenic initiation events, we performed the same analysis on a 1-kb region in each gene (see Fig. S4C at <http://goo.gl/OEGSsQ>). Here, we observed only a modest 3' enrichment, with no gene length dependence, suggesting that intragenic initiation sites are randomly distributed along genes of different sizes. Taken together, with the antisense results, these data suggest that, as in *S. cerevisiae* (29, 32), intragenic transcription is prevalent in an *spt6* mutant in *S. pombe*.

Finally, in addition to altered levels of annotated transcripts and identification of novel transcripts, we observed novel splice events in the *spt6-1* mutant. By a conservative estimate, we observed 374 novel splicing events in the *spt6-1* mutant that do not occur in either the wild-type sample or the reference genome (Fig. 3A; see also Table S5 at <http://goo.gl/OEGSsQ>). A subset of these events ($n = 81$) represents novel splice sites within annotated transcription units. Given the similar number ($n = 53$) of sense splice sites that were identified specifically in WT strains, the novel sense splice events are not likely due to *spt6-1* specific splicing events, but missing annotations due to low signal. On the other hand, the remaining 293 splicing events occur in previously unannotated antisense ($n = 222$) or intergenic ($n = 71$) transcripts (Fig. 3A); for example, transcripts antisense to the *pop1⁺* and *puc1⁺* genes are spliced (Fig. 3B). We compared the splice sites from all of these different classes and found that, overall, the novel transcripts are spliced at sequences similar to those observed in standard coding genes in a WT strain; for example, the consensus donor, acceptor, and branch sites for the *spt6-1* specific antisense introns are very similar to those observed in WT introns (Fig. 3C). These results suggest that the high occurrence of novel splice events in the *spt6-1* mutant is likely due to production of novel antisense and intergenic transcripts, which are then properly processed. Taken together, the transcriptional data indicate that Spt6 is critical for transcriptional accuracy genome-wide, particularly for preventing transcription and processing of both intragenic and intergenic transcripts on a global level.

Nucleosome positions are globally disrupted in an *spt6* mutant. Spt6 has previously been shown to control chromatin structure in *S. cerevisiae* (12, 18, 19, 29, 55). These results, combined with the widespread transcriptional changes in the *spt6-1* mutant,

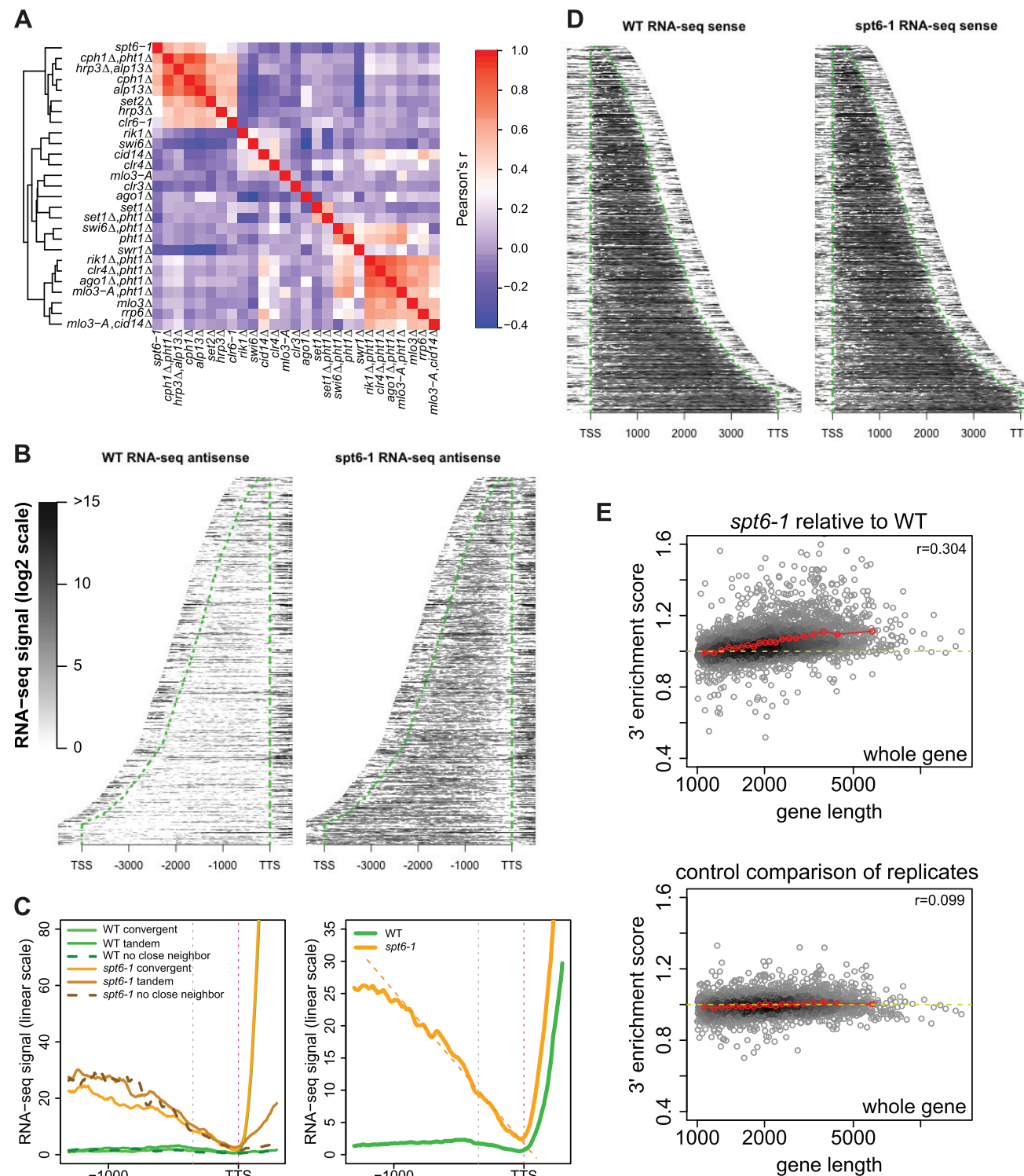


FIG 2 Spt6 is required for the repression of cryptic intragenic transcripts on the sense and antisense strands. (A) RNA-seq data was clustered with previous tiling microarray data to determine similarity of antisense profiles of each mutant. The heat map is colored by Pearson correlation value (see Table S4 at <http://goo.gl/OEGSsQ>) and clustered by similarity. (B) Heat maps display the \log_2 expression values on the antisense strand of each transcription unit, sorted by size and aligned by the TTS on the sense strand (vertical green line). The curved green line represents the TSS on the sense strand. (C) Metagene analysis of the RNA-seq antisense signal upstream of the TTS binned by convergent genes, tandem genes, and genes with no neighbor within 0.5 kb (left panel) and for all loci (right panel), with the dashed orange line indicating a linear increase. The vertical dotted lines represent the TTS (pink) and 350 bp (gray). (D) Heat maps display \log_2 expression values on the sense strand at each transcription unit sorted by size and aligned by TSS. (E) Three prime enrichment scores were calculated for all genes comparing WT to *spt6-1* (top panel) or comparing the first and second replicates as a control, each pooling WT and *spt6-1* (bottom panel). Enrichment scores for each transcription unit were plotted by the length of the gene and the red dots represent the averages of 20 bins by length, each containing 5% of the transcripts.

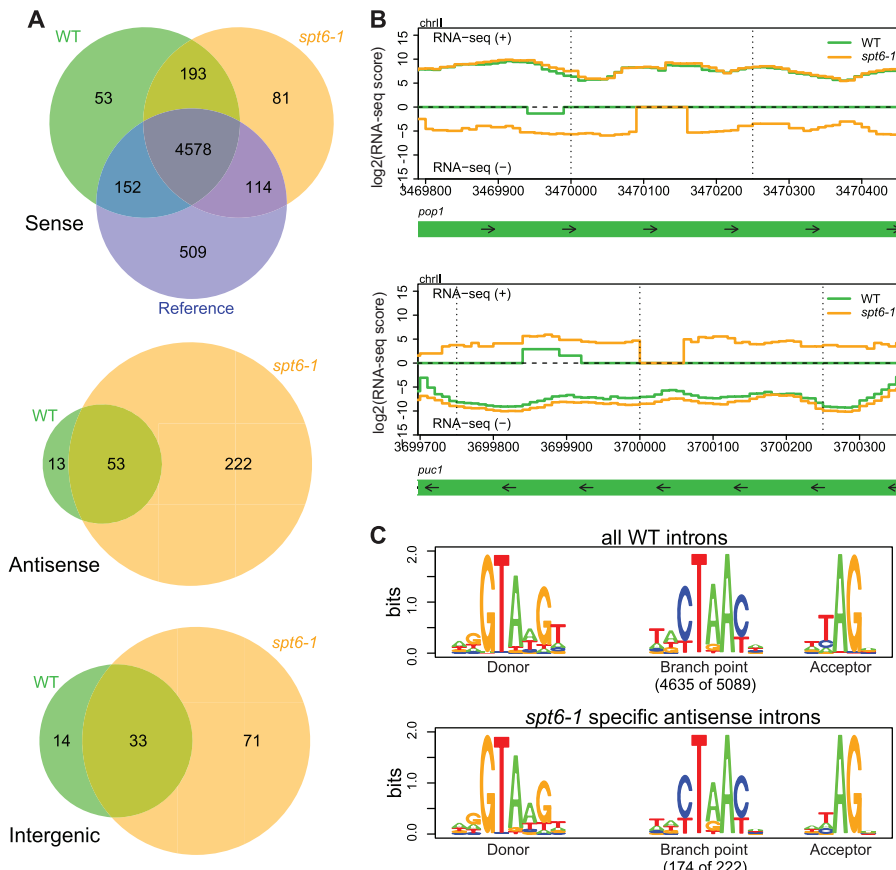


FIG 3 Antisense and intergenic transcripts are spliced. (A) Venn diagrams showing the overlap between splicing events in WT and the *spt6-1* mutant. Splicing events were called for all cases where >50% of the reads mapped to the exon-exon junction in both WT or *spt6-1* RNA-seq repeats. The occurrence of WT and *spt6-1* splice sites were compared for sense, antisense, and intergenic transcripts. Sense transcripts were also compared to the reference genome annotation. (B) The *pop1* (top panel) and *puc1* (bottom panel) antisense transcripts are spliced, as shown by the $\log_2(\text{RNA-seq scores})$, plotted on the plus (positive values) and minus (negative values) strands. (C) Sequence logos of the donor, acceptor, and branch points were determined for all WT introns and *spt6-1* specific antisense introns. The branch point was identified manually and was found in 4,635/5,089 and 174/222 introns, respectively; these introns were used to calculate the sequence logo.

prompted us to investigate this requirement for Spt6 in *S. pombe*. We used MNase digestion followed by high-throughput sequencing (MNase-seq), as well as ChIP-seq of histones H2B and H3, to assess nucleosome positioning and occupancy in the *spt6-1* mutant. Metagene analysis of the MNase-seq results revealed that nucleosome occupancy is drastically perturbed over both promoter and coding regions in the *spt6-1* mutant, with nucleosome phasing altered over the coding regions (Fig. 4A). Our histone ChIP-seq results showed that nucleosome loss occurs over transcribed regions in the *spt6-1* mutant (Fig. 4B; see also Fig. S5A and B at <http://goo.gl/OEGSsQ>), with this effect dominated by loss over highly transcribed genes (Fig. 4C; see also Fig. S5B at <http://goo.gl/OEGSsQ>). These results are consistent with previous studies which indicate that Spt6 is important for histone maintenance primarily over highly transcribed genes (19). Overall, we found that nucleosome positioning and occupancy is substantially perturbed in the *spt6-1* mutant, suggesting that Spt6 plays an important role in maintaining the normal nucleosome state.

Spt6 is required for two widespread histone modifications, H3K4me3 and H3K36me3. Two histone modifications, H3K4me3 and H3K36me3, correlate with active transcription over 5' and 3' transcribed regions, respectively (for a review, see

reference 63). Interestingly, recent studies have suggested that Spt6 is required for H3K4me3 in humans (37) but not in *S. cerevisiae* (M. Murawska and F. Winston, unpublished data). In contrast, past studies have shown that Spt6 is required for normal levels of H3K36 methylation in both mammalian cells and *S. cerevisiae* (25–28). To test whether Spt6 regulates these modifications in *S. pombe*, we first used Western blotting to assess the levels of these histone modifications in both WT and *spt6-1* strains. Our results demonstrate a dramatic loss of both H3K4me3 and H3K36me3 in the *spt6-1* mutant (Fig. 5A, compare lanes 1 and 2). The level of these histone modifications in the *spt6-1* mutant appears equivalent to that in strains deleted for the responsible methyltransferases, *set1Δ* and *set2Δ*, respectively (Fig. 5A, compare lanes 2, 6, and 7). While this work was in progress, another study also showed that H3K4me3 is Spt6 dependent (33).

In other organisms, both H3K4me3 and H3K36me3 are dependent upon the Paf1 complex (for a review, see reference 64). Furthermore, previous studies in *S. cerevisiae* have suggested functional interactions between Paf1 and Spt6 (24). To test whether the H3 methylation defects we observed are caused by reduced Paf1 complex recruitment in an *spt6-1* mutant, we measured Paf1 recruitment by ChIP-seq of the Ctr9 subunit. Our results show

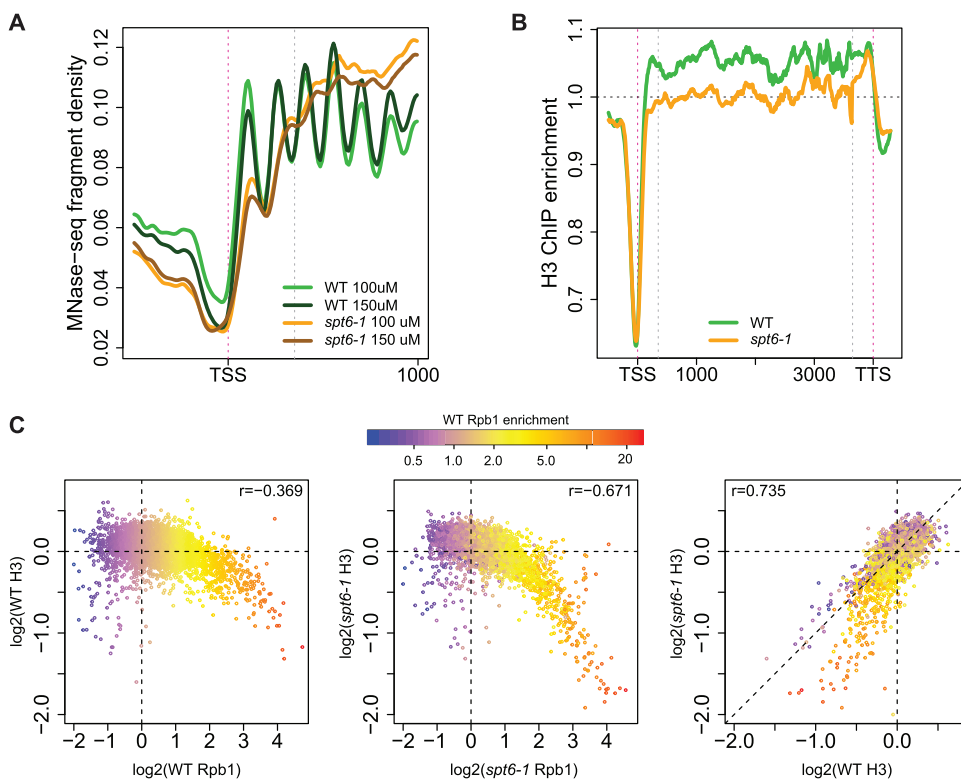


FIG 4 Spt6 regulates nucleosome positioning and occupancy at transcribed regions. (A) Metagene analysis shows nucleosome positioning in WT and *spt6-1* strains over transcribed regions aligned to the TSS, as determined by MNase-seq analysis using two concentrations of MNase (100 and 150 μ M). The vertical dotted lines represent the TSS and TTS (pink) and 350 bp (gray). (B) Metagene analysis shows H3 enrichment by ChIP-seq over transcribed regions in WT and *spt6-1* strains aligned to the TSS and TTS. (C) The log₂ ChIP-seq enrichment scores for Rpb1 and H3 at each transcription unit are plotted in WT (left panel) and *spt6-1* (center panel), and the log₂ ChIP enrichment scores for H3 are plotted for WT and *spt6-1* strains (right panel). All plots are colored by enrichment of WT Rpb1 as an indicator of transcriptional activity, and *r* values correspond to the Pearson correlation.

that Ctr9 was enriched over transcribed regions as expected but that there was decreased recruitment in the *spt6-1* mutant compared to the WT (Fig. 5B), in spite of unchanged Ctr9 protein levels (see Fig. S5C at <http://goo.gl/OEGSsQ>). To investigate whether this decreased recruitment accounts for the loss of either

H3K4me3 or H3K36me3, we measured these histone modifications in two different Paf1 mutants (*paf1* Δ and *rtf1* Δ). In *S. cerevisiae*, H3K4me3 is dependent upon both Paf1 and Rtf1 (65, 66), whereas H3K36me3 is dependent upon Paf1 but not Rtf1 (67). As expected, both *paf1* Δ and *rtf1* Δ mutants are defective for H3K4me3. However, unexpectedly, both mutants displayed normal levels of H3K36me3 (Fig. 5A). This result suggests that in *S. pombe*, H3K36me3 is Paf1-independent and that the loss of H3K36me3 in the *spt6-1* mutant is not caused by reduced Paf1 recruitment.

The Paf1 complex controls H3K4me3 by promoting ubiquitylation of H2B (H2BK119ub in *S. pombe*), since this modification is required to recruit the COMPASS complex, which contains Set1 and is required for H3K4me3 (68–73). To determine whether Spt6 promotes H3K4me3 via this pathway, we measured H2BK119ub levels. Our results confirm that H2BK119ub is undetectable in the *paf1* Δ and *rtf1* Δ mutants, but surprisingly, we found that it is present in the *spt6-1* mutant (Fig. 5A, compare lanes 1 through 4). Deletion of the gene encoding the E2 ubiquitin ligase for H2B, *rhp6* $^+$, causes loss of both H2BK119ub and H3K4me3 (Fig. 5A, lane 5), confirming that the dependence of H3K4me3 on H2BK119ub is conserved in *S. pombe*. Our results strongly suggest that, as for K36me3, Spt6 is required for H3K4me3 by a mechanism distinct from Paf1.

Spt6 regulates H3K4me3 by promoting recruitment of the COMPASS complex. Since H3K4me3 is dependent on Spt6 in

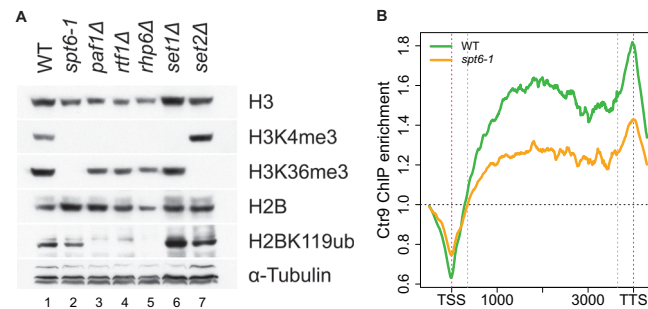


FIG 5 Spt6 regulates H3K4me3 and H3K36me3 independently of the Paf1 complex. (A) Western blots were used to measure histone modifications in WT, *spt6-1*, and Paf1 complex mutants (*paf1* Δ and *rtf1* Δ), as well as control strains for each mark: *rhp6* Δ (H2BK119ub), *set1* Δ (H3K4me3), and *set2* Δ (H3K36me3). Western blotting was performed with antibodies to H3, H3K4me3, H3K36me3, H2B, H2BK119ub, and α -tubulin as a loading control. (B) Metagene analysis shows the ChIP-seq enrichment of Ctr9 (Paf1 complex) in WT and *spt6-1* strains over transcribed regions aligned to the TSS and the TTS. The vertical dotted lines represent the TSS and TTS (pink) and 350 bp (gray).

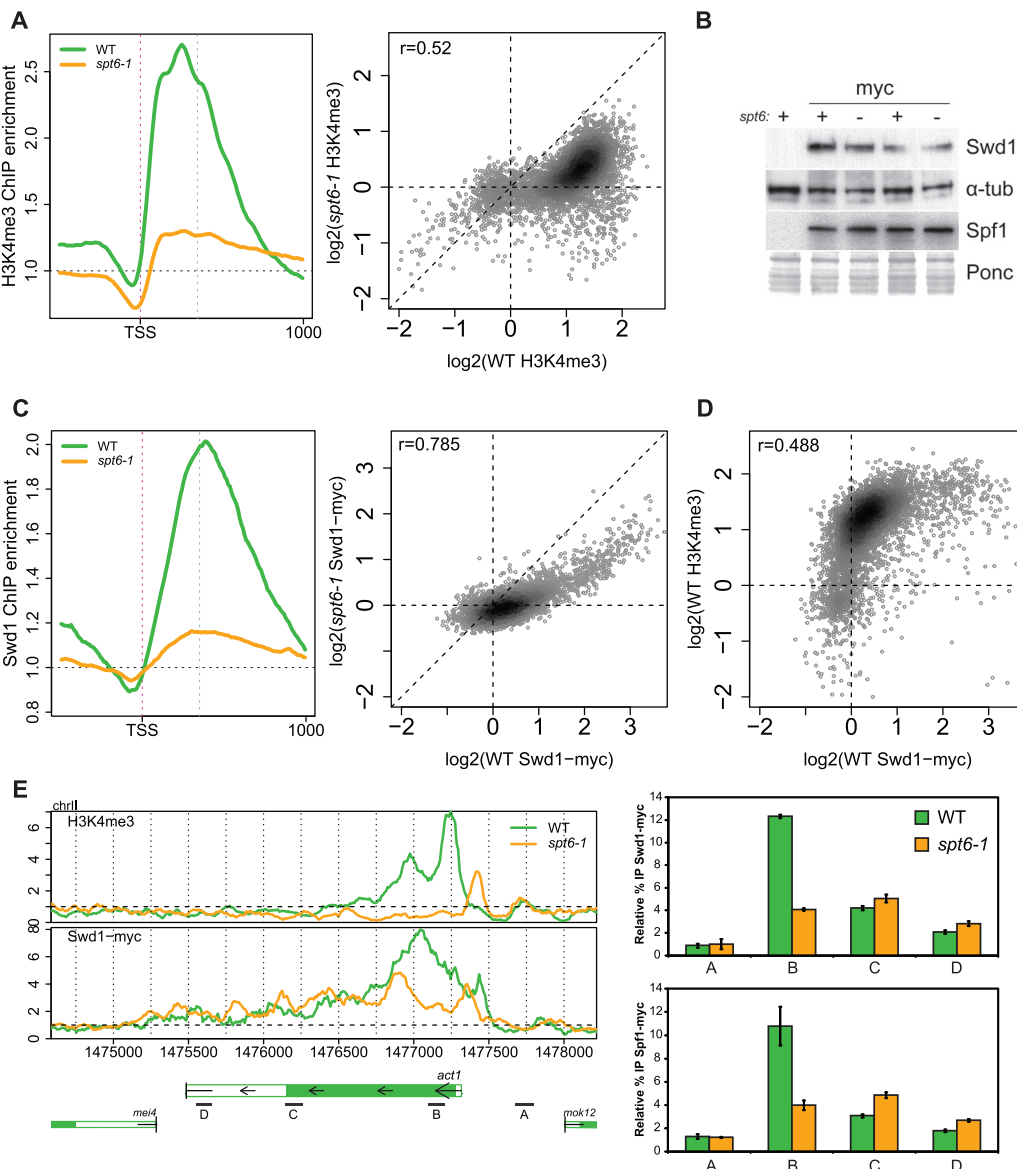


FIG 6 Spt6 is required for H3K4me3 and COMPASS recruitment. (A) ChIP-seq enrichment of H3K4me3 in WT and *spt6-1* strains over transcribed regions is shown as a metagene aligned to the TSS (left panel) and in \log_2 scale on a scatter plot (right panel). The vertical dotted lines represent the TSS (pink) and 350 bp (gray). (B) Western blots show protein levels of two myc-tagged components of the COMPASS complex, Swd1 and Spf1, in two biological replicates of WT and *spt6-1* strains using the anti-myc antibody, with α -tubulin or Ponceau serving as a loading control. (C) ChIP-seq enrichment of the Swd1 subunit of COMPASS in WT and *spt6-1* strains over transcribed regions is shown as a metagene aligned to the TSS and TTS (left panel) and in \log_2 scale on a scatter plot (right panel). (D) WT \log_2 ChIP-seq enrichment scores for Swd1 and H3K4me3 at each transcription unit. (E) Comparison of ChIP-seq (left panel) and directed ChIP qPCR (right panels) of COMPASS binding at *act1*⁺. qPCR was performed at four regions of *act1*⁺ as indicated by the black bars and labeled A to D in the left panel. Enrichment of the Swd1 (right, top) and Spf1 (right, bottom) COMPASS subunits were assessed in WT and *spt6-1* strains, with enrichment normalized to a gene free region. Columns represent the mean \pm the SEM ($n = 3$ to 4). ChIP-seq enrichment values of H3K4me3 and Swd1 over the *act1*⁺ region are shown in the left panel.

human cells but not in *S. cerevisiae*, *S. pombe* can serve as a model system for studying this Spt6 dependency. We performed ChIP-seq of H3K4me3 to assess its distribution genome-wide in WT and *spt6-1* strains. As expected, H3K4me3 was enriched at the 5' ends of genes in WT strains, but it was greatly reduced over this region in the *spt6-1* mutant (Fig. 6A). We considered that this defect might be an indirect transcriptional effect of *spt6-1* on one or more genes encoding components of the COMPASS complex. However, based on our RNA-seq data, we did not observe signif-

icant changes to these genes in the *spt6-1* mutant (see Table S6 at <http://goo.gl/OEGSsQ>); additionally, we measured the protein levels of the COMPASS components Swd1 and Spf1 and found that they are unaffected in the *spt6-1* mutant (Fig. 6B). Thus, the H3K4me3 defect in *spt6-1* is unlikely to be caused by reduced COMPASS levels.

To determine whether COMPASS recruitment is impaired in an *spt6-1* mutant, we performed ChIP-seq with Swd1 and found a pattern similar to that of H3K4me3; there is an enrichment of

Swd1 over the 5' ends of genes in the wild-type strain, and this level is greatly reduced in the *spt6-1* mutant (Fig. 6C). In the WT, we observed a binary pattern with all genes above a certain level of COMPASS having similar levels of H3K4me3 and genes below it lacking H3K4me3 (Fig. 6D). In the *spt6-1* mutant, recruitment of Swd1 drops below this threshold at many genes, suggesting that this decreased recruitment of COMPASS could explain the loss of H3K4me3. We verified our ChIP-seq by targeted ChIP at *act1⁺* and observed an equivalent decrease in 5' end recruitment of Swd1 and Spf1 in the *spt6-1* mutant (Fig. 6E), suggesting that the recruitment of the entire COMPASS complex, rather than a specific subunit, is affected. Our results suggest that this recruitment defect is not due to a defect in the Paf1 complex or H2B ubiquitylation (Fig. 5A) but that H3K4me3 is reduced in the *spt6-1* mutant due to reduced recruitment of COMPASS through another mechanism.

Spt6 is required for optimal recruitment of Set2, the H3K36 methyltransferase. We then took similar approaches to examine the loss of H3K36me3 in the *spt6-1* mutant. First, we performed H3K36me3 ChIP-seq in both WT and *spt6-1* strains. As expected, in the WT strain, we observed a strong signal over the gene body, except for the 5' end (Fig. 7A); however, we were unable to collect sufficient material from the IP in the *spt6-1* mutant to build a library for ChIP-seq, a finding consistent with the undetectable levels by Western blotting (Fig. 5A, lane 2). We therefore performed gene-specific ChIP, which requires less starting material, to assess H3K36me3 levels at *act1⁺* and observed that H3K36me3 was undetectable in the *spt6-1* mutant, equivalent to the levels seen in a *set2Δ* mutant (Fig. 7B, top panel). These results strongly suggest that H3K36me3 is completely abolished in the *spt6-1* mutant. In an *S. cerevisiae spt6-1004* mutant, the defect in H3K36me3 is partly due to decreased protein levels of Set2 (28); however, we found that Set2 levels are normal in the *S. pombe spt6-1* mutant (Fig. 7C). To test whether Set2 recruitment is Spt6 dependent, we performed Set2 ChIP-seq and found that Set2 recruitment was modestly decreased in the *spt6-1* mutant compared to the WT (Fig. 7D and E). We confirmed this result by directed ChIP at *act1⁺* (Fig. 7B). In WT strains, Spt6 and Set2 binding is highly correlated at transcribed regions genome-wide (Fig. 7F), indicating that they associate similarly with RNAPII. Taken together, these results suggest that Spt6 is required for optimal recruitment of Set2 to elongating RNAPII and that the decreased recruitment in the *spt6-1* mutant may contribute to the loss of H3K36me3.

DISCUSSION

Our results suggest that Spt6 is a master regulator of transcription, chromatin structure, and histone modifications across the genome (Fig. 8). In an *spt6* mutant, there are striking changes to transcription, including changes to the levels and start sites of mRNAs, a global increase in antisense transcript levels, and evidence of intragenic transcription initiation on both the sense and the antisense strands. In addition, nucleosome positioning is greatly altered, with decreased occupancy over both promoters and coding regions, and highly disrupted phasing. Finally, two widespread histone modifications, H3K4me3 and H3K36me3, are substantially lost, which is likely due, at least in part, to reduced recruitment of their methyltransferases. All of these effects may be direct, given the previously established direct interactions of Spt6 with both RNAPII and histones.

Our results support a model in which Spt6 is required for mul-

tiple mechanisms for the repression of antisense transcription. Previous studies have shown that several distinct classes of factors are required for antisense repression in *S. pombe*, including the Chd chromatin remodelers, Hrp1 and Hrp3, the H3K36 methyltransferase, Set2, the histone variant H2A.Z, the RNAi machinery, and the exosome (45–47, 57–61). Similar to *S. pombe*, Set2 and the remodelers Chd1 and Isw1 are required for antisense repression in *S. cerevisiae* (55, 74). The pattern of antisense transcripts in an *S. pombe spt6* mutant is most similar to those of mutants in the Clr6 complex, as well as the *in set2Δ* and *hrp3Δ* mutants. Although it is difficult to compare results from our RNA-seq experiments to the microarray experiments of the other studies due to differences in the dynamic range (see Fig. S4A at <http://goo.gl/OEGSsQ>), the very large number of loci with increased antisense levels in the *spt6* mutant suggests a more extensive defect than in either *set2Δ* or *hrp3Δ*. Furthermore, Spt6 has been functionally linked to the RNAi machinery (34) and the exosome (75), both of which control antisense transcripts at the posttranscriptional level (46, 57), indicating that it could also play a role in the repression of read-through transcription at convergent genes. However, our results indicate that the majority of the antisense transcripts in an *spt6* mutant initiate from within genes. An understanding of the regulation of these antisense promoters by Spt6 and their possible biological roles are important issues for future studies.

Spt6 is a histone chaperone, proposed to replace nucleosomes in the wake of transcription by RNAPII, and loss of this histone chaperone activity in an *spt6* mutant could explain the loss of nucleosome occupancy and phasing over transcribed regions. This would also be consistent with highly transcribed regions displaying stronger defects. Nucleosome occupancy has previously been examined in several mutants in *S. pombe* and *S. cerevisiae*. In particular, the defects observed in the *spt6* mutant look similar to those in mutants lacking the Chd chromatin remodelers in both yeasts (45, 58, 60, 76), suggesting that there may be some interplay between Spt6 and Chd remodelers. Further studies will be necessary to determine whether Spt6 has any role in the recruitment or function of these remodelers, or whether they control chromatin structure via independent mechanisms.

Our studies of H3K4me3 in an *S. pombe spt6-1* mutant have highlighted several interesting issues. First, the dependency of H3K4me3 on Spt6 differs between organisms, since the modification is Spt6 dependent in both *S. pombe* (33; the present study) and humans (37) but is Spt6 independent in *S. cerevisiae* (Murawska and Winston, unpublished). The difference between *S. pombe* and *S. cerevisiae* is unlikely to be caused by different *spt6* alleles since the two alleles we used, *spt6-1* in *S. pombe* and *spt6-1004* in *S. cerevisiae*, both delete the region encoding the Spt6 helix-hairpin-helix motif. Second, in the *S. pombe spt6-1* mutant, the level of the COMPASS complex appears to be normal, and yet its recruitment is severely reduced genome-wide, providing an explanation for the H3K4me3 defect. The recruitment defect is not understood, although it could be caused by the chromatin changes in an *spt6-1* mutant. A recent study (33) provided evidence that histone turnover is elevated in *S. pombe spt6* mutants and suggested that this might affect histone modifications. Third, the loss of H3K4me3 allows us to observe another interesting difference between *S. cerevisiae* and *S. pombe*. A previous study demonstrated that in *S. cerevisiae*, H3K4me3 was required for the initiation of some repressive antisense transcripts at the 3' ends of genes (77); however, this does not seem to be a global phenomenon in *S. pombe*, since

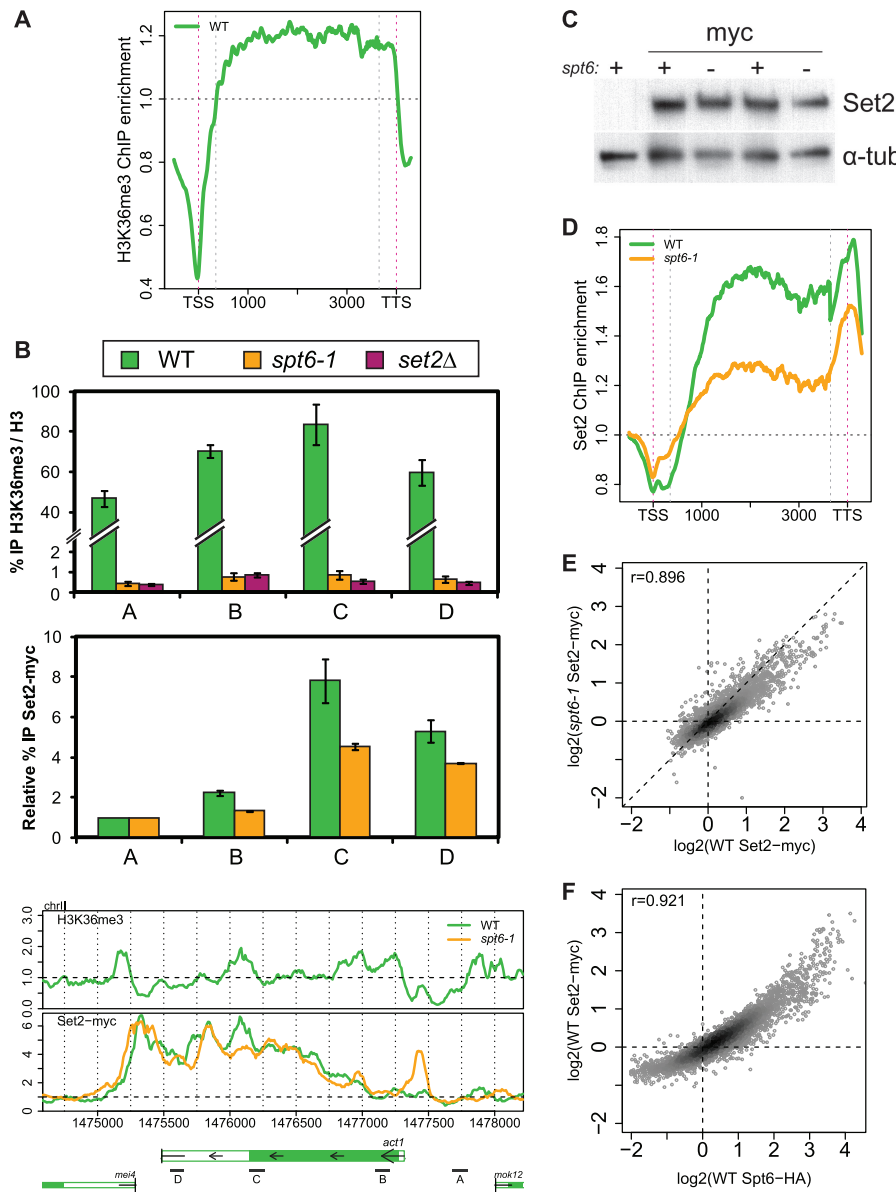


FIG 7 Spt6 is required for H3K36me3 and contributes to Set2 recruitment. (A) Metagene analysis shows H3K36me3 ChIP-seq enrichment over transcribed regions, aligned to the TSS and TTS, in WT cells. No results are shown for the *spt6-1* strain since the IP did not produce enough material for sequencing due to the low level of H3K36me3. The vertical dotted lines represent the TSS and TTS (pink) and 350 bp (gray). (B) Comparison of directed ChIP qPCR (top and middle panels) and ChIP-seq (bottom panel) of H3K36me3 and Set2 at *act1*⁺. qPCR was performed at four regions of *act1*⁺ indicated by the black bars and labeled A to D. For H3K36me3, modification levels were normalized to H3 levels at each primer set, and at Set2, primer sets were normalized to the upstream, untranscribed region (A). Columns represent the mean \pm the SEM ($n = 3$). ChIP-seq enrichment values over the *act1*⁺ region are shown in the bottom panel. (C) Set2 protein levels were measured by Western blots in WT and *spt6-1* strains with the anti-myc antibody, with α -tubulin serving as a loading control. (D) Metagene analysis shows enrichment of Set2 in wild-type and *spt6-1* strains over transcribed regions aligned to the TSS and TTS. (E) The \log_2 ChIP-seq enrichment scores for Set2 at each transcription unit are plotted in WT and *spt6-1* with r corresponding to the Pearson correlation. (F) The WT \log_2 ChIP-seq enrichment scores are plotted for Spt6 and Set2 at each transcription unit with r corresponding to the Pearson correlation.

we see widespread elevation of antisense transcript levels from the 3' ends of genes in *spt6-1* mutants, even though H3K4me3 is absent. Finally, the H3K4me3 defect in an *S. pombe* *spt6-1* mutant does not occur via an effect on H2B ubiquitylation. For all of these reasons, we believe that *S. pombe* provides an interesting system for studying the relationship between Spt6 and H3K4me3.

The Spt6 dependency of H3K36me3 appears to be more universal than for H3K4me3, since it has now been demonstrated in

S. pombe (our work), *S. cerevisiae* (25, 26, 28), and human cells (27). In *S. cerevisiae*, an *spt6* mutation causes decreased levels of Set2 (28), which we did not observe in *S. pombe*. We note, however, that when *S. cerevisiae* Set2 levels were increased to wild-type (WT) levels, this did not restore H3K36me3 (28), indicating additional defects in H3K36me3 in the *S. cerevisiae* *spt6* mutant. Previous studies suggest that many protein-protein interactions are required for both Set2 recruitment and activity, some of which

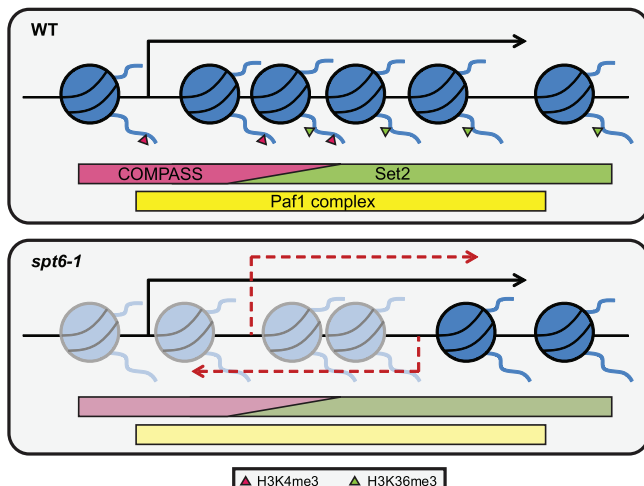


FIG 8 Spt6 is required for transcriptional accuracy and chromatin integrity. In WT strains (top panel), nucleosomes are organized across transcribed regions, with histone H3 trimethylated on K4 at the 5' end and K36 at the 3' end. These marks are deposited through recruitment of the COMPASS complex and Set2, respectively. Paf1 is also recruited and is required for H3K4me3 independently of Spt6. In the *spt6-1* mutant (bottom panel), nucleosome occupancy and positioning is compromised, and both H3 K4 and K36 trimethylation are lost, possibly due to decreased recruitment of COMPASS and Set2. Recruitment of the Paf1 complex is also decreased. In addition to the compromised chromatin state, intragenic transcripts initiate in both the sense and the antisense direction.

might be impaired or altered in an *spt6* mutant. These include interactions between Set2 and the RNAPII CTD (78–83), as well as Set2 and the Spt6-interacting partner Iws1/Spn1 (27). Other studies have shown that H3K36me2 and H3K36me3 are both dependent upon Set2 interactions with specific regions of histones H2A, H3, and H4 (84–86). Interestingly, histone or Set2 mutants that abolish the Set2-histone interaction still allow Set2 recruitment, but not H3K36me2 or H3K36me3, and they also mimic several *spt6* mutant phenotypes. Finally, we found that in *S. pombe*, surprisingly, H3K36me3 is independent of the Paf1 complex, in contrast to a strong dependence in *S. cerevisiae* (67).

In summary, Spt6 plays a number of important and interrelated roles in the regulation of transcription and chromatin, many of which may be direct, based on its interactions with RNAPII and histones. Now that the broad requirements for Spt6 have been more comprehensively defined, the challenge will be to elucidate the biochemical basis for each, as well as its functional role *in vivo*. Given the conservation of Spt6 and its central roles in gene expression and development, this understanding should provide additional insights into the integrated action of the large number of factors that operate during transcription.

ACKNOWLEDGMENTS

We thank Koon Ho Wong for his help and advice with the ChIP-seq experiments, Dom Helmlinger and Dan Spatt for helpful scientific discussions, and Dan S. Day for helpful comments on the manuscript.

This study was supported by a Wellcome Trust Senior Investigator Award (grant 095598/Z/11/Z) to J.B. and National Institutes of Health grant GM32967 to F.W.

REFERENCES

- Kung JT, Colognori D, Lee JT. 2013. Long noncoding RNAs: past, present, and future. *Genetics* 193:651–669.
- Harries LW. 2012. Long non-coding RNAs and human disease. *Biochem Soc Trans*. 40:902–906.
- Tisseur M, Kwapisz M, Morillon A. 2011. Pervasive transcription: lessons from yeast. *Biochimie* 93:1889–1896.
- Clark-Adams CD, Winston F. 1987. The SPT6 gene is essential for growth and is required for delta-mediated transcription in *Saccharomyces cerevisiae*. *Mol Cell Biol*. 7:679–686.
- Neigeborn L, Celenza JL, Carlson M. 1987. SSN20 is an essential gene with mutant alleles that suppress defects in SUC2 transcription in *Saccharomyces cerevisiae*. *Mol Cell Biol*. 7:672–678.
- Johnson SJ, Close D, Robinson H, Vallet-Gely I, Dove SL, Hill CP. 2008. Crystal structure and RNA binding of the Tex protein from *Pseudomonas aeruginosa*. *J Mol Biol*. 377:1460–1473.
- Close D, Johnson SJ, Sdano MA, McDonald SM, Robinson H, Formosa T, Hill CP. 2011. Crystal structures of the *Saccharomyces cerevisiae* Spt6 core and C-terminal tandem SH2 domain. *J Mol Biol*. 408:697–713.
- Diebold ML, Loeliger E, Koch M, Winston F, Cavarelli J, Romier C. 2010. Noncanonical tandem SH2 enables interaction of elongation factor Spt6 with RNA polymerase II. *J Biol Chem*. 285:38389–38398.
- Liu J, Zhang J, Gong Q, Xiong P, Huang H, Wu B, Lu G, Wu J, Shi Y. 2011. Solution structure of tandem SH2 domains from Spt6 protein and their binding to the phosphorylated RNA polymerase II C-terminal domain. *J Biol Chem*. 286:29218–29226.
- Sun M, Lariviere L, Dengl S, Mayer A, Cramer P. 2010. A tandem SH2 domain in transcription elongation factor Spt6 binds the phosphorylated RNA polymerase II C-terminal repeat domain (CTD). *J Biol Chem*. 285:41597–41603.
- Yoh SM, Cho H, Pickle L, Evans RM, Jones KA. 2007. The Spt6 SH2 domain binds Ser2-P RNAPII to direct Iws1-dependent mRNA splicing and export. *Genes Dev*. 21:160–174.
- Bortvin A, Winston F. 1996. Evidence that Spt6 controls chromatin structure by a direct interaction with histones. *Science* 272:1473–1476.
- Winkler M, aus Dem Siepen T, Stamminger T. 2000. Functional interaction between pleiotropic transactivator pUL69 of human cytomegalovirus and the human homolog of yeast chromatin regulatory protein SPT6. *J Virol*. 74:8053–8064.
- Diebold ML, Koch M, Loeliger E, Cura V, Winston F, Cavarelli J, Romier C. 2010. The structure of an Iws1/Spt6 complex reveals an interaction domain conserved in TFIIS, Elongin A, and Med26. *EMBO J*. 29:3979–3991.
- Pujari V, Radebaugh CA, Chodaparambil JV, Muthurajan UM, Almeida AR, Fischbeck JA, Luger K, Stargell LA. 2010. The transcription factor Spn1 regulates gene expression via a highly conserved novel structural motif. *J Mol Biol*. 404:1–15.
- Chen S, Ma J, Wu F, Xiong LJ, Ma H, Xu W, Lv R, Li X, Villen J, Gygi SP, Liu XS, Shi Y. 2012. The histone H3 Lys 27 demethylase JMJD3 regulates gene expression by impacting transcriptional elongation. *Genes Dev*. 26:1364–1375.
- Wang AH, Zare H, Mousavi K, Wang C, Moravec CE, Sirotkin HI, Ge K, Gutierrez-Cruz G, Sartorelli V. 2013. The histone chaperone Spt6 coordinates histone H3K27 demethylation and myogenesis. *EMBO J*. 32:1075–1086.
- Adkins MW, Tyler JK. 2006. Transcriptional activators are dispensable for transcription in the absence of Spt6-mediated chromatin reassembly of promoter regions. *Mol Cell* 21:405–416.
- Ivanovska I, Jacques PE, Rando OJ, Robert F, Winston F. 2011. Control of chromatin structure by *spt6*: different consequences in coding and regulatory regions. *Mol Cell Biol*. 31:531–541.
- Jensen MM, Christensen MS, Bonven B, Jensen TH. 2008. Requirements for chromatin reassembly during transcriptional downregulation of a heat shock gene in *Saccharomyces cerevisiae*. *FEBS J*. 275:2956–2964.
- Ardehali MB, Yao J, Adelman K, Fuda NJ, Petesch SJ, Webb WW, Lis JT. 2009. Spt6 enhances the elongation rate of RNA polymerase II *in vivo*. *EMBO J*. 28:1067–1077.
- Endoh M, Zhu W, Hasegawa J, Watanabe H, Kim DK, Aida M, Inukai N, Narita T, Yamada T, Furuya A, Sato H, Yamaguchi Y, Mandal SS, Reinberg D, Wada T, Handa H. 2004. Human Spt6 stimulates transcription elongation by RNA polymerase II *in vitro*. *Mol Cell Biol*. 24:3324–3336.
- Bucheli ME, Buratowski S. 2005. Npl3 is an antagonist of mRNA 3' end formation by RNA polymerase II. *EMBO J*. 24:2150–2160.
- Kaplan CD, Holland MJ, Winston F. 2005. Interaction between tran-

- scription elongation factors and mRNA 3'-end formation at the *Saccharomyces cerevisiae* GAL10-GAL7 locus. *J. Biol. Chem.* 280:913–922.
25. Carrozza MJ, Li B, Florens L, Suganuma T, Swanson SK, Lee KK, Shia WJ, Anderson S, Yates J, Washburn MP, Workman JL. 2005. Histone H3 methylation by Set2 directs deacetylation of coding regions by Rpd3S to suppress spurious intragenic transcription. *Cell* 123:581–592.
 26. Chu Y, Sutton A, Sternglanz R, Prelich G. 2006. The BUR1 cyclin-dependent protein kinase is required for the normal pattern of histone methylation by SET2. *Mol. Cell. Biol.* 26:3029–3038.
 27. Yoh SM, Lucas JS, Jones KA. 2008. The Iws1:Spt6:CTD complex controls cotranscriptional mRNA biosynthesis and HYPB/Setd2-mediated histone H3K36 methylation. *Genes Dev.* 22:3422–3434.
 28. Youdell ML, Kizer KO, Kisileva-Romanova E, Fuchs SM, Duro E, Strahl BD, Mellor J. 2008. Roles for Ctk1 and Spt6 in regulating the different methylation states of histone H3 lysine 36. *Mol. Cell. Biol.* 28: 4915–4926.
 29. Kaplan CD, Laprade L, Winston F. 2003. Transcription elongation factors repress transcription initiation from cryptic sites. *Science* 301: 1096–1099.
 30. Formosa T, Ruone S, Adams MD, Olsen AE, Eriksson P, Yu Y, Rhoades AR, Kaufman PD, Stillman DJ. 2002. Defects in SPT16 or POB3 (yFACT) in *Saccharomyces cerevisiae* cause dependence on the Hir/Hpc pathway: polymerase passage may degrade chromatin structure. *Genetics* 162: 1557–1571.
 31. Hartzog GA, Wada T, Handa H, Winston F. 1998. Evidence that Spt4, Spt5, and Spt6 control transcription elongation by RNA polymerase II in *Saccharomyces cerevisiae*. *Genes Dev.* 12:357–369.
 32. Cheung V, Chua G, Batada NN, Landry CR, Michnick SW, Hughes TR, Winston F. 2008. Chromatin- and transcription-related factors repress transcription from within coding regions throughout the *Saccharomyces cerevisiae* genome. *PLoS Biol.* 6:e277. doi:[10.1371/journal.pbio.0060277](https://doi.org/10.1371/journal.pbio.0060277).
 33. Kato H, Okazaki K, Iida T, Nakayama J, Murakami Y, Urano T. 2013. Spt6 prevents transcription-coupled loss of posttranslationally modified histone H3. *Sci. Rep.* 3:2186.
 34. Kiely CM, Marguerat S, Garcia JF, Madhani HD, Bahler J, Winston F. 2011. Spt6 is required for heterochromatic silencing in the fission yeast *Schizosaccharomyces pombe*. *Mol. Cell. Biol.* 31:4193–4204.
 35. Nishiwaki K, Sano T, Miwa J. 1993. emb-5, a gene required for the correct timing of gut precursor cell division during gastrulation in *Caenorhabditis elegans*, encodes a protein similar to the yeast nuclear protein SPT6. *Mol. Gen. Genet.* 239:313–322.
 36. Keegan BR, Feldman JL, Lee DH, Koos DS, Ho RK, Stainier DY, Yelon D. 2002. The elongation factors Pandora/Spt6 and Foggy/Spt5 promote transcription in the zebrafish embryo. *Development* 129:1623–1632.
 37. Begum NA, Stanlie A, Nakata M, Akiyama H, Honjo T. 2012. The histone chaperone Spt6 is required for activation-induced cytidine deaminase target determination through H3K4me3 regulation. *J. Biol. Chem.* 287:32415–32429.
 38. Gallastegui E, Millan-Zambrano G, Terme JM, Chavez S, Jordan A. 2011. Chromatin reassembly factors are involved in transcriptional interference promoting HIV latency. *J. Virol.* 85:3187–3202.
 39. Nakamura M, Basavarajah P, Rousset E, Beraud C, Latreille D, Henaoui IS, Lassot I, Mari B, Kiernan R. 2012. Spt6 levels are modulated by PAAF1 and proteasome to regulate the HIV-1 LTR. *Retrovirology* 9:13.
 40. Forsburg SL, Rhind N. 2006. Basic methods for fission yeast. *Yeast* 23: 173–183.
 41. Bahler J, Wu JQ, Longtine MS, Shah NG, McKenzie A, III, Steever AB, Wach A, Philipsen P, Pringle JR. 1998. Heterologous modules for efficient and versatile PCR-based gene targeting in *Schizosaccharomyces pombe*. *Yeast* 14:943–951.
 42. Edgar R, Domrachev M, Lash AE. 2002. Gene Expr. Omnibus: NCBI gene expression and hybridization array data repository. *Nucleic Acids Res.* 30:207–210.
 43. Lyne R, Burns G, Mata J, Penkett CJ, Rustici G, Chen D, Langford C, Vetrie D, Bahler J. 2003. Whole-genome microarrays of fission yeast: characteristics, accuracy, reproducibility, and processing of array data. *BMC Genomics* 4:27. doi:[10.1186/1471-2164-4-27](https://doi.org/10.1186/1471-2164-4-27).
 44. Trapnell C, Pachter L, Salzberg SL. 2009. TopHat: discovering splice junctions with RNA-Seq. *Bioinformatics* 25:1105–1111.
 45. Shim YS, Choi Y, Kang K, Cho K, Oh S, Lee J, Grewal SI, Lee D. 2012. Hrp3 controls nucleosome positioning to suppress non-coding transcription in eu- and heterochromatin. *EMBO J.* 31:4375–4387.
 46. Zhang K, Fischer T, Porter RL, Dhakshnamoorthy J, Zofall M, Zhou M, Veenstra T, Grewal SI. 2011. Clr4/Suv39 and RNA quality control factors cooperate to trigger RNAi and suppress antisense RNA. *Science* 331: 1624–1627.
 47. Zofall M, Fischer T, Zhang K, Zhou M, Cui B, Veenstra TD, Grewal SI. 2009. Histone H2A.Z cooperates with RNAi and heterochromatin factors to suppress antisense RNAs. *Nature* 461:419–422.
 48. Bailey TL, Boden M, Buske FA, Frith M, Grant CE, Clementi L, Ren J, Li WW, Noble WS. 2009. MEME SUITE: tools for motif discovery and searching. *Nucleic Acids Res.* 37:W202–W208.
 49. Garcia JF, Dumesic PA, Hartley PD, El-Samad H, Madhani HD. 2010. Combinatorial, site-specific requirement for heterochromatic silencing factors in the elimination of nucleosome-free regions. *Genes Dev.* 24: 1758–1771.
 50. Helmlinger D, Marguerat S, Villen J, Gygi SP, Bahler J, Winston F. 2008. The *S. pombe* SAGA complex controls the switch from proliferation to sexual differentiation through the opposing roles of its subunits Gcn5 and Spt8. *Genes Dev.* 22:3184–3195.
 51. Shin JA, Choi ES, Kim HS, Ho JC, Watts FZ, Park SD, Jang YK. 2005. SUMO modification is involved in the maintenance of heterochromatin stability in fission yeast. *Mol. Cell* 19:817–828.
 52. Langmead B, Trapnell C, Pop M, Salzberg SL. 2009. Ultrafast and memory-efficient alignment of short DNA sequences to the human genome. *Genome Biol.* 10:R25.
 53. Cheung MS, Down TA, Latorre I, Ahringer J. 2011. Systematic bias in high-throughput sequencing data and its correction by BEADS. *Nucleic Acids Res.* 39:e103.
 54. Kharchenko PV, Tolstorukov MY, Park PJ. 2008. Design and analysis of ChIP-seq experiments for DNA-binding proteins. *Nat. Biotechnol.* 26: 1351–1359.
 55. van Bakel H, Tsui K, Gebbia M, Mnaimneh S, Hughes TR, Nislow C. 2013. A compendium of nucleosome and transcript profiles reveals determinants of chromatin architecture and transcription. *PLoS Genet.* 9:e1003479. doi:[10.1371/journal.pgen.1003479](https://doi.org/10.1371/journal.pgen.1003479).
 56. Anderson HE, Wardle J, Korkut SV, Murton HE, Lopez-Maury L, Bahler J, Whitehall SK. 2009. The fission yeast HIRA histone chaperone is required for promoter silencing and the suppression of cryptic antisense transcripts. *Mol. Cell* 29:5158–5167.
 57. Buhler M, Spies N, Bartel DP, Moazed D. 2008. TRAMP-mediated RNA surveillance prevents spurious entry of RNAs into the *Schizosaccharomyces pombe* siRNA pathway. *Nat. Struct. Mol. Biol.* 15:1015–1023.
 58. Hennig BP, Bendrin K, Zhou Y, Fischer T. 2012. Chd1 chromatin remodelers maintain nucleosome organization and repress cryptic transcription. *EMBO Rep.* 13:997–1003.
 59. Nicolas E, Yamada T, Cam HP, Fitzgerald PC, Kobayashi R, Grewal SI. 2007. Distinct roles of HDAC complexes in promoter silencing, antisense suppression and DNA damage protection. *Nat. Struct. Mol. Biol.* 14:372–380.
 60. Pointner J, Persson J, Prasad P, Norman-Axelsson U, Stralfors A, Khorosjutina O, Krietenstein N, Svensson JP, Ekwall K, Korber P. 2012. CHD1 remodelers regulate nucleosome spacing in vitro and align nucleosomal arrays over gene coding regions in *S. pombe*. *EMBO J.* 31:4388–4403.
 61. Yamane K, Mizuguchi T, Cui B, Zofall M, Noma K, Grewal SI. 2011. Asf1/HIRA facilitate global histone deacetylation and associate with HP1 to promote nucleosome occupancy at heterochromatic loci. *Mol. Cell* 41:56–66.
 62. Lickwar CR, Rao B, Shabalin AA, Nobel AB, Strahl BD, Lieb JD. 2009. The Set2/Rpd3S pathway suppresses cryptic transcription without regard to gene length or transcription frequency. *PLoS One* 4:e4886. doi:[10.1371/journal.pone.0004886](https://doi.org/10.1371/journal.pone.0004886).
 63. Smolle M, Workman JL. 2013. Transcription-associated histone modifications and cryptic transcription. *Biochim. Biophys. Acta* 1829:84–97.
 64. Tomson BN, Arndt KM. 2013. The many roles of the conserved eukaryotic Paf1 complex in regulating transcription, histone modifications, and disease states. *Biochim. Biophys. Acta* 1829:116–126.
 65. Krogan NJ, Dover J, Wood A, Schneider J, Heidt J, Boateng MA, Dean K, Ryan OW, Golshani A, Johnston M, Greenblatt JF, Shilatifard A. 2003. The Paf1 complex is required for histone H3 methylation by COMPASS and Dot1p: linking transcriptional elongation to histone methylation. *Mol. Cell* 11:721–729.
 66. Ng HH, Robert F, Young RA, Struhl K. 2003. Targeted recruitment of Set1 histone methylase by elongating Pol II provides a localized mark and memory of recent transcriptional activity. *Mol. Cell* 11:709–719.

67. Chu Y, Simic R, Warner MH, Arndt KM, Prelich G. 2007. Regulation of histone modification and cryptic transcription by the Bre1 and Paf1 complexes. *EMBO J.* 26:4646–4656.
68. Dover J, Schneider J, Tawiah-Boateng MA, Wood A, Dean K, Johnston M, Shilatifard A. 2002. Methylation of histone H3 by COMPASS requires ubiquitination of histone H2B by Rad6. *J. Biol. Chem.* 277:28368–28371.
69. Kim J, Roeder RG. 2009. Direct Bre1-Paf1 complex interactions and RING finger-independent Bre1-Rad6 interactions mediate histone H2B ubiquitylation in yeast. *J. Biol. Chem.* 284:20582–20592.
70. Ng HH, Dole S, Struhl K. 2003. The Rtf1 component of the Paf1 transcriptional elongation complex is required for ubiquitination of histone H2B. *J. Biol. Chem.* 278:33625–33628.
71. Sun ZW, Allis CD. 2002. Ubiquitination of histone H2B regulates H3 methylation and gene silencing in yeast. *Nature* 418:104–108.
72. Wood A, Schneider J, Dover J, Johnston M, Shilatifard A. 2003. The Paf1 complex is essential for histone monoubiquitination by the Rad6-Bre1 complex, which signals for histone methylation by COMPASS and Dot1p. *J. Biol. Chem.* 278:34739–34742.
73. Xiao T, Kao CF, Krogan NJ, Sun ZW, Greenblatt JF, Osley MA, Strahl BD. 2005. Histone H2B ubiquitylation is associated with elongating RNA polymerase II. *Mol. Cell. Biol.* 25:637–651.
74. Smolle M, Venkatesh S, Gogol MM, Li H, Zhang Y, Florens L, Washburn MP, Workman JL. 2012. Chromatin remodelers Isw1 and Chd1 maintain chromatin structure during transcription by preventing histone exchange. *Nat. Struct. Mol. Biol.* 19:884–892.
75. Andrusis ED, Werner J, Nazarian A, Erdjument-Bromage H, Tempst P, Lis JT. 2002. The RNA processing exosome is linked to elongating RNA polymerase II in *Drosophila*. *Nature* 420:837–841.
76. Gkikopoulos T, Schofield P, Singh V, Pinskaya M, Mellor J, Smolle M, Workman JL, Barton GJ, Owen-Hughes T. 2011. A role for Snf2-related nucleosome-spacing enzymes in genome-wide nucleosome organization. *Science* 333:1758–1760.
77. Margaritis T, Oreal V, Brabers N, Maestroni L, Vitaliano-Prunier A, Benschop JJ, van Hooff S, van Leenen D, Dargemont C, Geli V, Holstege FC. 2012. Two distinct repressive mechanisms for histone 3 lysine 4 methylation through promoting 3'-end antisense transcription. *PLoS Genet.* 8:e1002952. doi:[10.1371/journal.pgen.1002952](https://doi.org/10.1371/journal.pgen.1002952).
78. Kizer KO, Phatnani HP, Shibata Y, Hall H, Greenleaf AL, Strahl BD. 2005. A novel domain in Set2 mediates RNA polymerase II interaction and couples histone H3 K36 methylation with transcript elongation. *Mol. Cell. Biol.* 25:3305–3316.
79. Krogan NJ, Kim M, Tong A, Golshani A, Cagney G, Canadian V, Richards DP, Beattie BK, Emili A, Boone C, Shilatifard A, Buratowski S, Greenblatt J. 2003. Methylation of histone H3 by Set2 in *Saccharomyces cerevisiae* is linked to transcriptional elongation by RNA polymerase II. *Mol. Cell. Biol.* 23:4207–4218.
80. Li B, Gogol M, Carey M, Lee D, Seidel C, Workman JL. 2007. Combined action of PHD and chromo domains directs the Rpd3S HDAC to transcribed chromatin. *Science* 316:1050–1054.
81. Li B, Howe L, Anderson S, Yates JR, III, Workman JL. 2003. The Set2 histone methyltransferase functions through the phosphorylated carboxyl-terminal domain of RNA polymerase II. *J. Biol. Chem.* 278:8897–8903.
82. Schaft D, Roguev A, Kotovic KM, Shevchenko A, Sarov M, Neugebauer KM, Stewart AF. 2003. The histone 3 lysine 36 methyltransferase, SET2, is involved in transcriptional elongation. *Nucleic Acids Res.* 31:2475–2482.
83. Xiao T, Hall H, Kizer KO, Shibata Y, Hall MC, Borchers CH, Strahl BD. 2003. Phosphorylation of RNA polymerase II CTD regulates H3 methylation in yeast. *Genes Dev.* 17:654–663.
84. Du HN, Briggs SD. 2010. A nucleosome surface formed by histone H4, H2A, and H3 residues is needed for proper histone H3 Lys36 methylation, histone acetylation, and repression of cryptic transcription. *J. Biol. Chem.* 285:11704–11713.
85. Du HN, Fingerman IM, Briggs SD. 2008. Histone H3 K36 methylation is mediated by a trans-histone methylation pathway involving an interaction between Set2 and histone H4. *Genes Dev.* 22:2786–2798.
86. Psathas JN, Zheng S, Tan S, Reese JC. 2009. Set2-dependent K36 methylation is regulated by novel intratail interactions within H3. *Mol. Cell. Biol.* 29:6413–6426.